

RESEARCH ARTICLE

10.1002/2015JB012453

Key Points:

- Orogen-parallel anisotropy in the Cordilleran lower crust suggests pervasive deformation
- Weak azimuthal anisotropy in the Cordilleran asthenosphere due to vertical mantle flow
- Frozen lithospheric fabrics and flow-driven asthenospheric anisotropy beneath the craton

Supporting Information:

- Figures S1–S3

Correspondence to:

X. Bao,
xubao@ucalgary.ca

Citation:

Bao, X., D. W. Eaton, and Y. J. Gu (2016), Rayleigh wave azimuthally anisotropic phase velocity maps beneath western Canada, *J. Geophys. Res. Solid Earth*, 121, 1821–1834, doi:10.1002/2015JB012453.

Received 20 AUG 2015

Accepted 18 FEB 2016

Accepted article online 20 FEB 2016

Published online 12 MAR 2016

Rayleigh wave azimuthally anisotropic phase velocity maps beneath western Canada

Xuewei Bao¹, David W. Eaton¹, and Yu Jeffrey Gu²

¹Department of Geoscience, University of Calgary, Calgary, Alberta, Canada, ²Department of Physics, University of Alberta, Edmonton, Alberta, Canada

Abstract The lithospheric evolution of western Laurentia spans several billion years of Earth history and provides an exceptional opportunity for investigating continental deformation during Archean and Proterozoic assembly of the craton and subsequent Phanerozoic orogenic processes along its western margin. In this study we present fundamental-mode Rayleigh wave azimuthal anisotropy in the period range 20–150 s for western Laurentia and the southern Canadian Cordillera. The surface wave phase velocity maps offer new constraints on the depth distribution of seismic anisotropy in this region. At short periods (20–25 s), strong anisotropy with an orogen-parallel fast direction is evident in the Cordillera and neighboring foreland belt, suggesting pervasive ductile deformation in the lower crust during Laramide orogenesis. At periods of 70 s and higher, a zone of low-to-null azimuthal anisotropy is evident in the southern part of the Cordillera. This apparent null region is interpreted to reflect complex asthenospheric flow due to the combined effects of the Juan de Fuca slab window, lithospheric delamination, and small-scale edge-driven convection. Depth-variant azimuthal anisotropy is evident beneath the cratonic part of the study region. The dominant direction of fast wave propagation in the southeastern part of the craton changes from N-S at periods of <120 s to NE-SW at 150 s period. This depth dependence is inferred to arise from different origins of the observed anisotropy, with “frozen” anisotropy within cratonic lithosphere underlain by flow-driven anisotropy in the asthenosphere. The frozen N-S trending fabrics in the middle to lower cratonic lithosphere most likely reflect processes of Paleoproterozoic assembly of western Laurentia.

1. Introduction

The tectonic setting of western Canada is characterized by a transition from the Jurassic to Eocene Cordilleran orogen in the west to the Precambrian craton in the east (Figure 1), making this region an excellent natural laboratory to study continental lithospheric deformation in connection with cratonic assembly and orogenic evolution. The eastern part of our study region belongs to Laurentia, the continental nucleus of North America. Assembly of this part of Laurentia occurred circa 2.0–1.8 Ga through a series of complex processes involving plate collision and/or terrane accretion among the diverse domains [Hoffman, 1988; Ross, 2002]. Following the collisional assembly of these Precambrian domains, a thick Proterozoic passive-margin sequence developed along the western flank of Laurentia, which was further modified by tectonic accretion and orogenic activity in the Canadian Cordillera after the Jurassic [Cook, 1995].

Seismic anisotropy, the directional variation in seismic wave speed, can provide important clues about Earth's deep deformation. Shear wave splitting analysis is the most widely used seismological technique for investigating azimuthal anisotropy beneath continents [Savage, 1999; Silver, 1996]. This approach provides high lateral resolution but relatively poor vertical resolution due to the near-vertical paths of the core-refracted teleseismic arrivals. In some regions, the fast-propagation azimuths from shear wave splitting are parallel to regional tectonic structures, which are typically interpreted to indicate that splitting occurred within the lithosphere [Babuška and Plomerová, 2006; Bastow et al., 2007, 2011]. Other regions show coherent fast-propagation directions parallel to those of the absolute plate motion, suggesting a sublithospheric origin [Bokelmann and Silver, 2000; Eaton et al., 2004; Vinnik et al., 1992]. Surface waves can offer vertical resolution of the depth distribution of seismic anisotropy [Adam and Lebedev, 2012; Gaherty, 2004; Lebedev et al., 2009; Montagner and Tanimoto, 1991]. Global and continental scale tomographic models from surface wave modeling have revealed different patterns of azimuthal anisotropy in the continental lithosphere and asthenosphere [Debayle et al., 2005; Marone and Romanowicz, 2007; Montagner and Tanimoto, 1991; Yuan and Romanowicz, 2010]. Regional-scale investigations using surface wave data from broadband

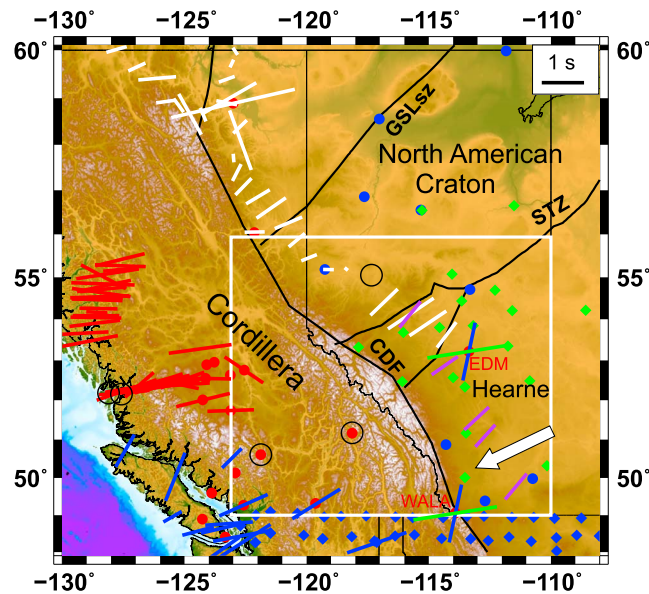


Figure 1. Topographic map of the study region with broadband seismic stations and SKS splitting measurements superimposed. The white box represents the area with good tomographic resolution. Blue dots are Alberta Telemetered Seismic Network, green diamonds are stations from CRANE array, red dots show Canadian National Seismic Network, and blue diamonds show stations from USArray. Short bars represent SKS splitting parameters (blue: Currie *et al.* [2004], red: Zandt *et al.* [2009], purple: Shragge *et al.* [2002], white: Courtier *et al.* [2010]). For stations WALA and EDM, the blue and green bars present the splitting parameters for the upper and lower anisotropic layers, respectively [Currie *et al.*, 2004]. Black circles denote null splitting measurements. White arrow indicates plate motion from no-net-rotation model [Gripp and Gordon, 2002]. CDF: Cordillera deformation front, GSLsz: Great Slave Lake shear zone, and STZ: Snowbird Tectonic Zone.

Kao *et al.*, 2013; Mercier *et al.*, 2009; Miller and Eaton, 2010; Nieuwenhuis *et al.*, 2014; Shragge *et al.*, 2002]. Ambient noise tomography and receiver functions have imaged large velocity gradients [Kao *et al.*, 2013], widespread low-velocity zones [Dalton *et al.*, 2011] and positive radial anisotropy ($\sim 4\text{--}5\%$) [Dalton and Gaherty, 2013] in the middle crust beneath the Canadian Cordillera on the west and complex crustal domains and evolution beneath western Laurentia to the east [Chen *et al.*, 2015b; Gu and Shen, 2015]. A sharp increase in lithospheric thickness from the Cordillera to the craton has been elucidated by *S* receiver functions [Miller and Eaton, 2010], teleseismic body wave tomography [Mercier *et al.*, 2009] and surface wave tomography [Bao *et al.*, 2014]. Furthermore, episodic development of the cratonic keel beneath Laurentia has been proposed by a number of investigators [Bao and Eaton, 2015; Boerner *et al.*, 1999; Nieuwenhuis *et al.*, 2014; Ross *et al.*, 2000; Shragge *et al.*, 2002].

To date, however, constraints from seismic anisotropy on deep lithospheric deformation of the region have been limited by relatively sparse SKS splitting observations [Courtier *et al.*, 2010; Currie *et al.*, 2004; Gu *et al.*, 2011; Shragge *et al.*, 2002; Zandt *et al.*, 2009]. A common feature of these studies is a predominance of fast splitting directions across western Laurentia that lie approximately parallel to the direction of absolute plate motion; superimposed on this pattern are small-scale variations in shear wave splitting that likely have a complex origin (Figure 1). For example, apparent null regions, characterized by a lack of a clear splitting signature, have been documented in the interior of the southern Canadian Cordillera and attributed to complex mantle flow in the back-arc region [Currie *et al.*, 2004; Zandt *et al.*, 2009]. Due to the limited vertical resolution of shear wave splitting observations, however, the preservation of fossil anisotropic fabrics that may be associated with assembly of the cratonic keel is unclear. Additional complications in the splitting patterns may also arise from mantle circulation patterns that are driven by subduction as well as small-scale

arrays, such as the present study, are producing increasingly high-resolution 3-D models of anisotropy and thus are significantly improving our understanding of continental deformation [Chen *et al.*, 2015a; Darbyshire *et al.*, 2013; Darbyshire and Lebedev, 2009; Fry *et al.*, 2010; Li *et al.*, 2003; Lin *et al.*, 2011; Pawlak *et al.*, 2012; Pedersen *et al.*, 2006; Yao *et al.*, 2010].

The lithospheric domains beneath the West Canada Sedimentary Basin (Figure 1) have been examined previously through analysis of regional gravity and magnetic data, seismic reflection and refraction profiles, and geochronological data [Ross *et al.*, 1991, 2000; Ross, 2002, and references therein]. These efforts are complemented by passive seismological studies and magnetotelluric surveys, which have provided additional constraints on the heterogeneities of the lithosphere-asthenosphere system beneath western Canada [Bao and Eaton, 2015; Bao *et al.*, 2014; Boerner *et al.*, 1999; Cassidy, 1995; Chen *et al.*, 2015b; Dalton and Gaherty, 2013; Dalton *et al.*, 2011; Gu and Shen, 2015; Gu *et al.*, 2015;

edge-driven convection caused by the sharp change of lithospheric thickness from the craton to the Cordillera [Bao *et al.*, 2014].

To address these issues, this study investigates azimuthally anisotropic Rayleigh wave phase velocity for western Canada using data from several recently deployed seismic networks to provide complementary information on the depth distribution of anisotropy in this region. Our model shows strong orogen-parallel anisotropy in the lower crust beneath the Cordillera and adjacent foreland belt, an apparent low-anisotropy region in the southern Cordilleran asthenosphere, and depth-variant anisotropy in the craton. Detailed interpretation of these structural features provides new insights into both Cordilleran orogenesis and the assembly of cratonic domains in western Canada.

2. Data Set and Tomographic Inversion

Fundamental-mode Rayleigh wave data utilized in this study are from 19 stations of the Canadian National Seismograph Network, 9 stations of the Alberta Telemetered Seismograph Network, 19 stations of the Canadian Rockies and Alberta Network (CRANE) [Gu *et al.*, 2011], and 39 stations from USArray (Figure 1). We selected 583 shallow and intermediate-focus events (depths < 100 km) in a distance range of 20°–120° with magnitude larger than 6 in the time period from 2006 to 2013. The interstation Rayleigh wave phase velocity dispersion curves were extracted from high-quality records using a cross-correlation method [Bao *et al.*, 2011; Yao *et al.*, 2006]. For each station pair, only earthquakes located within ±5° of the interstation great circle path were used to be compatible with the great circle assumption that is inherent in the two-station method. The two-station cross-correlation method minimizes both the influence of uncertain earthquake source parameters and the path effects between the source and receiver [Yao *et al.*, 2006]. By averaging the dispersion curves from multiple source regions for the same station pair, we reduced potential sources of error caused by off-great-circle propagation and scattering. Only dispersion data averaged from at least three different events and with standard deviation lower than 2.5% were used for the tomographic inversion. The number of Rayleigh wave phase velocity measurements varies with period, and a maximum of ~1400 paths were retained at 50 s period. Figure 2 shows the path distributions of interstation phase velocity measurements at several periods. For detailed descriptions of the data analysis the reader is referred to Bao and Eaton [2015] and Bao *et al.* [2014].

From the resulting dispersion data, we used a linearized 2-D inversion method [Bao *et al.*, 2013; Xu *et al.*, 2013] to construct phase velocity maps at 1° × 1° grid spacing for the study region. For each interstation path, the predicted frequency-dependent travel time $t(\omega)$ was obtained from the measured phase velocity distribution $c(\theta, \varphi, \omega)$

$$t(\omega) = \int c^{-1}(\theta, \varphi, \omega) ds, \quad (1)$$

where ω is frequency and θ, φ specify coordinates of the geographical points along the path. The inversion problem can be expressed in the form of $\mathbf{Gm} = \mathbf{d} + \mathbf{e}$, where \mathbf{d} contains the observed travel time residuals relative to the reference model (usually the average phase velocity at each period) and \mathbf{m} denotes the model parameters (isotropic phase velocities and azimuthally anisotropic coefficients). The sensitivity matrix \mathbf{G} is known from the forward problem. To estimate \mathbf{m} , we minimize the following objective function:

$$E = \|\mathbf{Gm} - \mathbf{d}\|^2 + \lambda^2 \|\mathbf{m}\|^2 + \phi^2 \|L\mathbf{m}\|^2. \quad (2)$$

The first term in equation (2) measures the data misfit, the second is a model regularization term, and the third term is a Laplacian smoothing constraint, where L is the 2-D finite-difference Laplacian operator, and λ and ϕ are the damping and smoothing factors, respectively. Regularization parameters were selected based on a series of tests. The parameter λ constrains the inversion in order to reduce deviation from the a priori velocity model, such that a large value of λ results in greater sensitivity to the initial model. Similarly, a larger ϕ results in a smoother model (small roughness of the model) and a reduced sensitivity to data misfit (Figures S1 and S2 in the supporting information). We selected values for λ and ϕ that appropriately balance the data misfit, model damping, and smoothness, and the main features of our model are robust with regard to appropriate regularizations used in the inversion (Figures S1 and S2). The resulting sparse system of equations was solved using the LSQR algorithm [Paige and Saunders, 1982].

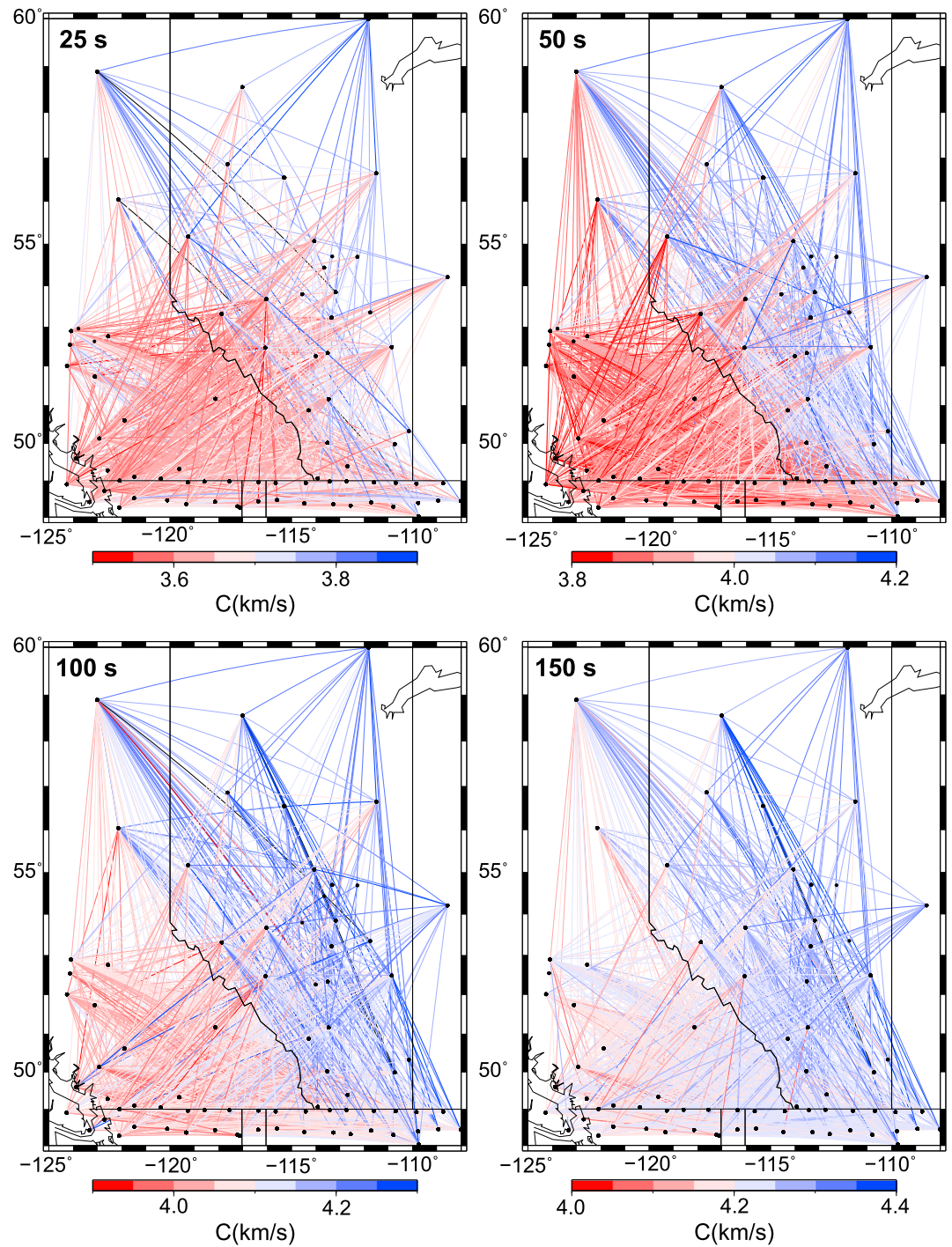
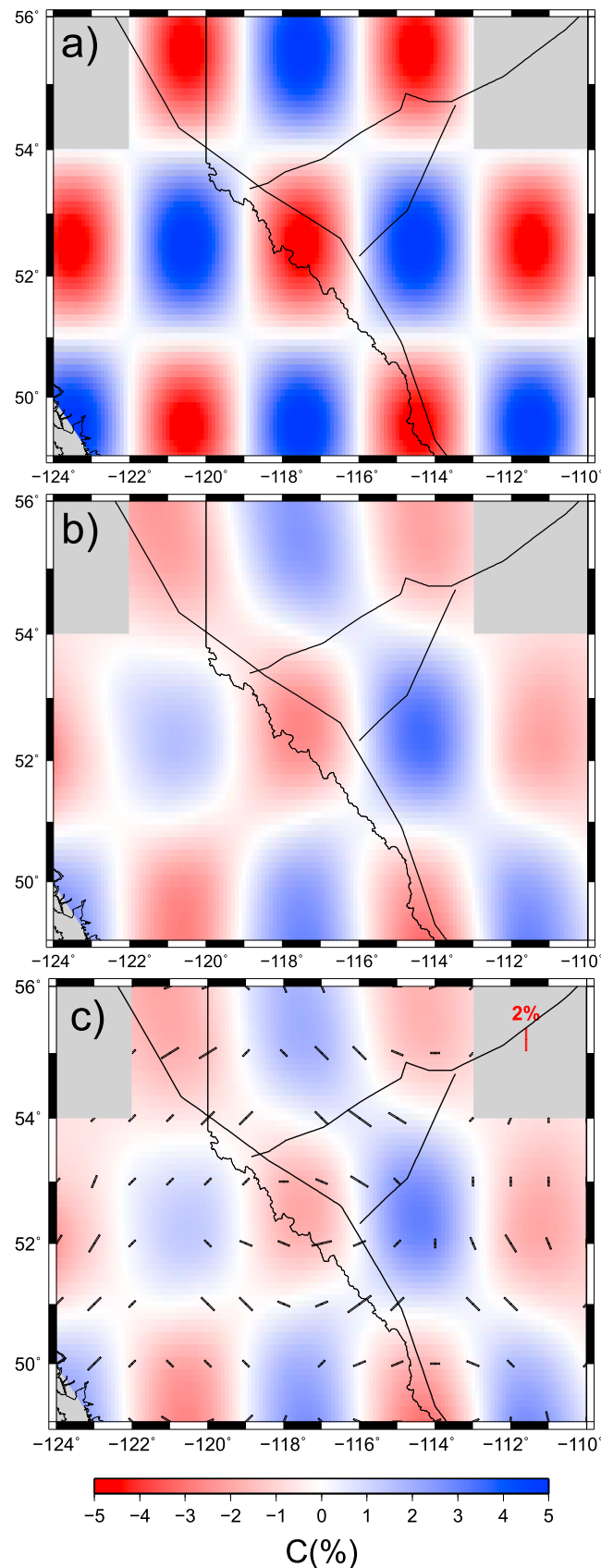


Figure 2. Path coverage of interstation phase velocity measurements at some representative periods. Color scale indicates phase velocity (C) variations.

To solve for azimuthal anisotropy, we can express Rayleigh wave phase velocity c as a function of azimuth ψ :

$$c(\theta, \phi, \omega) = A_0(\omega) + A_1(\omega) \cos(2\psi) + A_2(\omega) \sin(2\psi) + A_3(\omega) \cos(4\psi) + A_4(\omega) \sin(4\psi) \quad (3)$$

where A_0 is the azimuthal averaged phase velocity and A_1 – A_4 are azimuthal anisotropic coefficients [Smith and Dahlen, 1973]. The 4ψ terms are neglected, as they are generally very small [Li et al., 2003; Montagner



and Nataf, 1986; Yao et al., 2010]. The peak-to-peak amplitude of anisotropy is expressed as $2\sqrt{(A_1^2 + A_2^2)}/A_0$, and the fast wave propagation direction is represented as $\arctan(A_2/A_1)/2$.

3. Resolution and Leakage Tests

A series of synthetic tests were performed to evaluate the robustness of the anisotropic results. The regions north of 56°N and east of 110°W were not plotted in these tests due to the relatively sparse path coverage there. First, we created a purely isotropic checkerboard model, consisting of alternating positive and negative anomalies with respective magnitude of 5% above or below the average phase velocity at the corresponding period (Figure 3a). Synthetic phase velocity data were calculated according to the actual interstation path, and 2.5% random noise in phase velocity was added to mimic the errors in real data. These data were then used as input to the inversion procedure described above, including the use of the same damping and smoothing parameters as those for the real data. Figure 3b shows that the checkerboard velocity pattern is generally well recovered through an isotropic inversion, with the exception of clipped northeastern and northwestern segments. Another objective of this test is to evaluate the leakage of the input isotropic pattern into the recovered anisotropic velocity model. Model artifacts in the form of spurious anisotropy (<2% in magnitude) are mainly confined to areas of strong lateral velocity gradient (Figure 3c). Nevertheless, the leakage of isotropic velocity variation into ani-

Figure 3. Isotropic checkerboard reconstruction result for 50 s period. (a) The isotropic input model has ±5% peak-to-peak velocity variations. (b) Recovery of the synthetic model from isotropic inversion. (c) Result obtained from anisotropic inversion of the synthetic data. Some leakage is evident; spurious anisotropy is generally weak (<2%) and is oriented perpendicular to zones of high lateral velocity gradient.

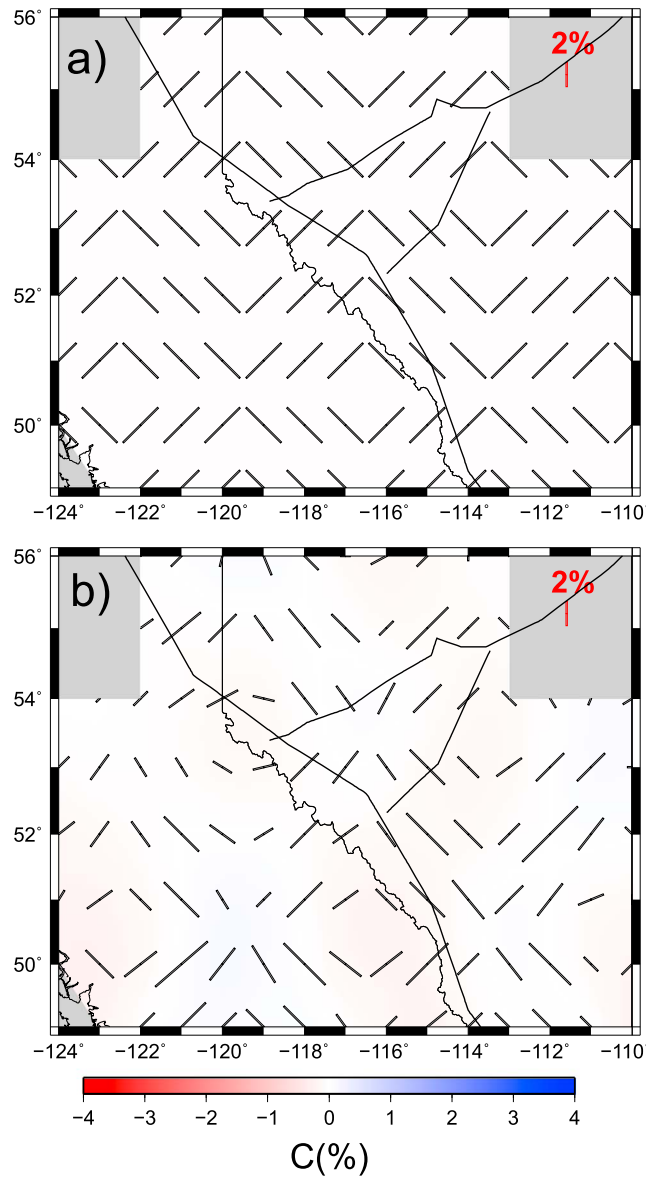


Figure 4. Anisotropic checkerboard reconstruction for 50 s period. (a) Input checkerboard model of azimuthal anisotropy with the average phase velocity at 50 s used as the homogeneous isotropic velocity. (b) Recovered model of azimuthal anisotropy. See supporting information for similar tests at other periods.

clear that the artificial anisotropy caused by the leakage of the isotropic heterogeneity shows localized variations, in contrast to the generally smooth distributions of anisotropy in our final models.

4. Results

Figure 6 shows azimuthally anisotropic phase velocity maps at periods from 25 to 150 s, which are sensitive to the velocity structure in an approximate depth range from the lower crust to the uppermost mantle (Figure 7). Throughout the period range considered here, a prominent feature of the isotropic velocity distribution is a pronounced structural transition from the high velocities within the craton in the northeast to the much lower velocities beneath the Cordillera in the southwest. The highest velocities appear in the Hearne domain, corresponding to a thickened cratonic keel imaged by previous studies [Gu and Shen, 2015; Bao and Eaton, 2015; Shragge et al., 2002]. This regional pattern of isotropic velocity distribution is similar to previous models

sotropic parameters means that caution should be exercised in the interpretation of results, particular in areas of strong lateral velocity gradient.

Second, a checkerboard anisotropic model was created with the fast azimuthal axis oriented NE–SW and NW–SE and the average phase velocity at a particular period as in the homogeneous isotropic velocity, from which synthetic phase velocity data were calculated. The anisotropic patterns for Rayleigh waves are generally well recovered, as shown in Figure 4. The deviations of anisotropic patterns from those of the input model are mainly related to sharp variations of anisotropic orientations. To examine further the robustness of the models and the leakage between isotropic and anisotropic structure, we took a phase velocity map obtained from the Rayleigh wave data set at a period of 70 s (see below), removed either the isotropic or anisotropic part (Figures 5a and 5b), and then reinverted it. The amplitude of isotropic and anisotropic patterns is generally well recovered (Figures 5c and 5d), and the azimuthal difference between the input and output models is less than 15° (Figure 5d). Reconstruction results also show that, in general, the leakage between isotropic phase velocity and anisotropic parameters is small (Figure 5c). The 7% peak-to-peak isotropic wave speed variation across the entire study region generated artificial peak-to-peak anisotropy of less than 0.9% that is confined to limited regions. It is also

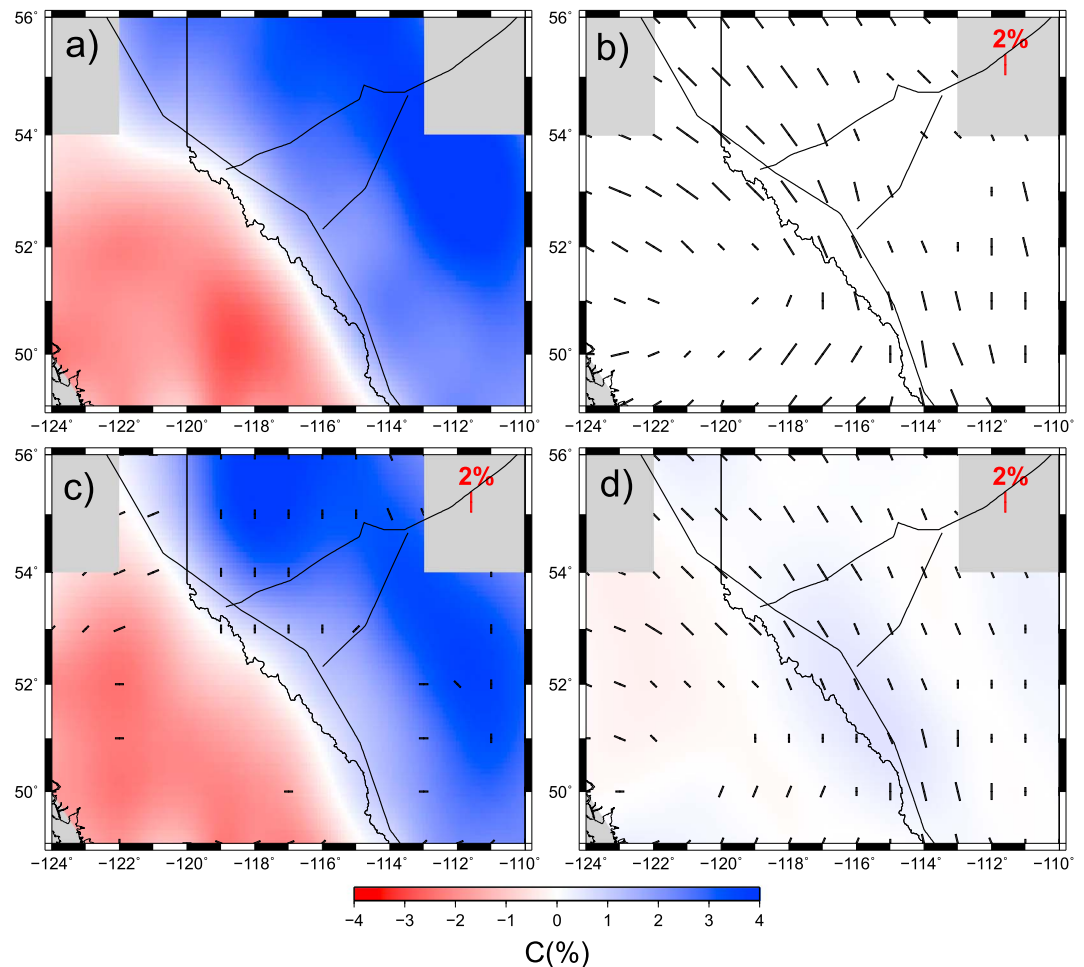
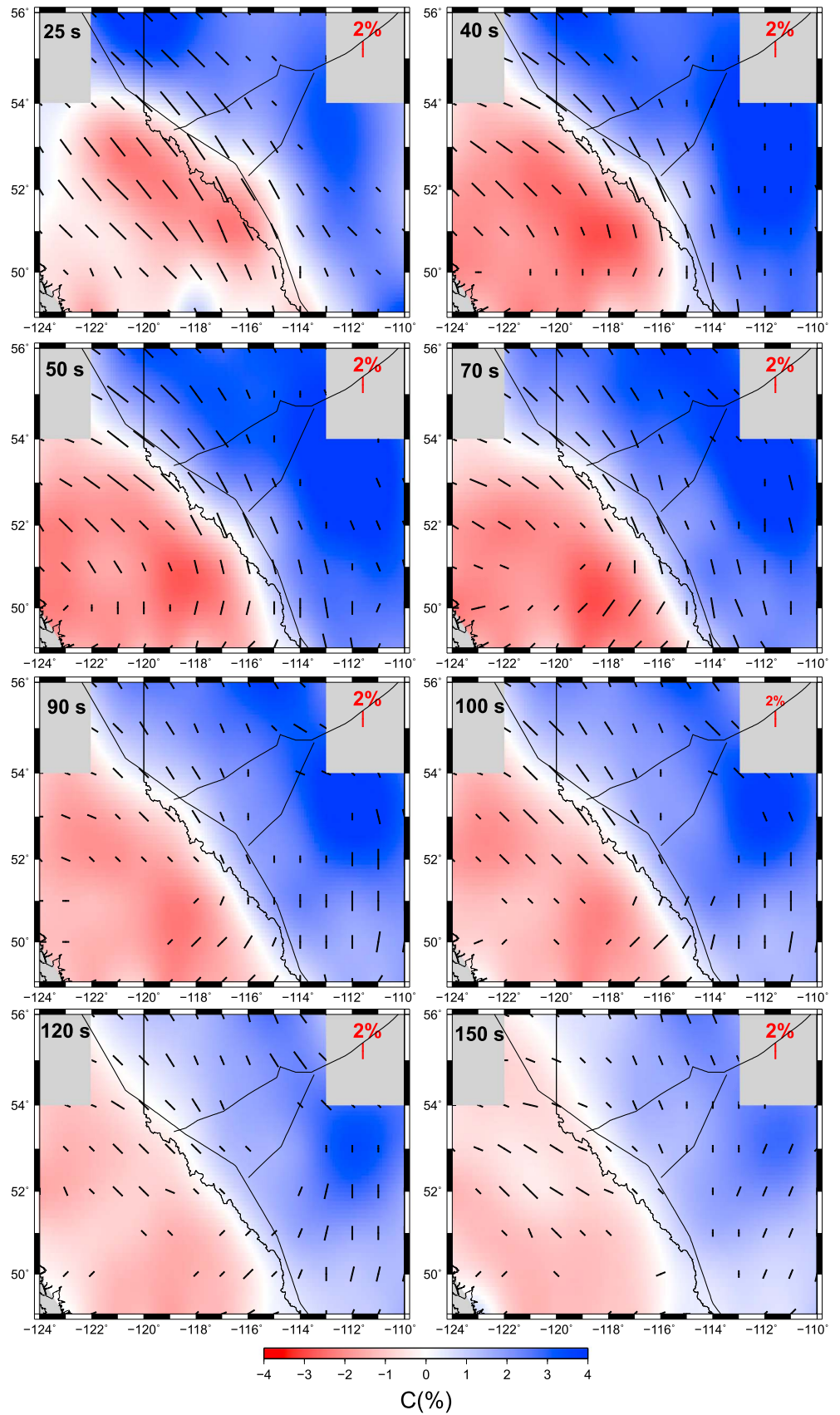


Figure 5. Leakage tests based on phase velocity map at 70 s period. (a) Original isotropic phase velocity map; (b) initial purely anisotropic phase velocity map; (c) result from the isotropic component; and (d) result from the anisotropic component (c). See text for details.

from isotropic tomography inversion [Bao and Eaton, 2015; Bao et al., 2014], suggesting that the isotropic phase velocities are not strongly influenced by the inclusion of azimuthal anisotropy in the inversion procedure. The generally coherent pattern of anisotropic fabric is markedly dissimilar to artifacts arising from spurious anisotropy that appear in our isotropic checkerboard test, providing confidence for interpretation of these results. The anisotropic inversion generally improves the fit to the measured travel times by ~10% compared to isotropic inversion, indicative of the relative significance of anisotropy in the inversion.

Figure 6 also displays pronounced variations of azimuthal anisotropy with period in our model. At short periods (25 s) that primarily sample the lower crust (Figure 7), we observe an orogen-parallel fast direction (nearly NW–SE) in the Canadian Cordillera and the neighboring foreland belt, where the peak-to-peak magnitude of anisotropy is the strongest (up to 4%). However, the intensity of azimuth anisotropy diminishes toward the interior of the craton at this period, forming a zone of low-to-null azimuthal anisotropy. At intermediate periods (40 s and 50 s), which primarily sample the uppermost mantle, the eastern part of the craton is characterized by relatively weak anisotropy, trending in an N-S fast-propagation direction. At these periods, the southern part of the Canadian Cordillera shows a noticeable decrease in the amplitude of anisotropy and change of the fast Rayleigh wave fast direction to NE–SW. At long periods (70 s and 90 s), the peak-to-peak anisotropy increases to 2.0%–2.5% in the southeastern craton region, reflecting stronger shear velocity azimuthal anisotropy in the deep part of the cratonic lithosphere. The relatively strong N-S trending azimuthal anisotropy of the southeastern craton persists to periods of 100 and 120 s, corresponding to the depth range of the middle to lower lithosphere under the craton. On the other hand, a zone of



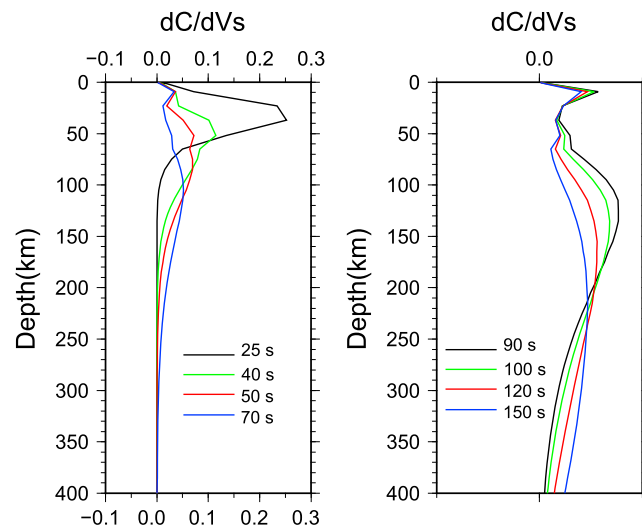


Figure 7. Rayleigh wave phase velocity sensitivity kernels for different period waves. The kernels are the partial derivatives for Rayleigh wave phase velocity with respect to V_s based on the velocity model (52°N, –112°W) obtained from *Bao and Eaton* [2015].

low-to-zero azimuthal anisotropy appears in the southern Canadian Cordillera at periods of 70 s and more. At 150 s period, which is sensitive to the conditions in the asthenosphere beneath the craton, the fast-propagation directions in the southeastern craton rotate into a NE-SW orientation.

5. Discussion

The nature of continental deformation at different depth ranges remains contentious even after decades of research. Here we consider two end-member models that describe the lithospheric evolution of continental regions. The first is a rigid block model [Tapponnier *et al.*, 1982; Tapponnier *et al.*, 2001], in which most deformation occurs along major boundary faults with little deformation in the interior of the blocks themselves.

In the opposite extreme, continental deformation may be considered as quasi-continuous [England and Houseman, 1986; Molnar, 1988], resulting from the ductile flow of a viscous sheet. Although the surficial movements of regions undergoing active deformation are increasingly well constrained using Global Positioning System observations, a conclusive discrimination between these two end-members remains elusive [Meade, 2007; Zhang *et al.*, 2004]. Deformation in the deep lithosphere is less well understood largely due to the lack of direct constraints, which is a key reason that measurements of seismic anisotropy is crucial within this depth range.

In response to sustained tectonic strains over long periods of geological time, intrinsically anisotropic crustal (e.g., mica and amphibole) and mantle (e.g., olivine and pyroxene) minerals may form preferred alignments that give rise to the detectable seismic anisotropy [Crampin *et al.*, 1984; Silver, 1996]. Azimuthal anisotropy is evident in various types of seismic data [Forsyth, 1975; Montagner and Tanimoto, 1991; Nataf *et al.*, 1984; Plomerová *et al.*, 2002; Savage, 1999; Shearer and Orcutt, 1986], and the fast direction of wave propagation has been widely used as an indicator of the directions of maximum deformation during the past and more recent tectonic events [Bystricky *et al.*, 2000; Nicolas and Christensen, 1987; Zhang and Karato, 1995]. Within the lithospheric mantle, lattice preferred orientation (LPO) of olivine is often attributed to “frozen” fabrics formed by past deformation processes [Ismail and Mainprice, 1998], whereas in the underlying asthenosphere seismic anisotropy is usually related to present and recent mantle flow [Adam and Lebedev, 2012; Deschamps *et al.*, 2008; Marone and Romanowicz, 2007; Yuan and Romanowicz, 2010]. However, in some cases, such as the presence of water or partial melt, the relationship between anisotropic fast direction and deformation could be more complex, and the interpretation of seismic anisotropy is more challenging [Bascou *et al.*, 2008; Holtzman *et al.*, 2003; Jung and Karato, 2001].

5.1. Strong Orogen-Parallel Anisotropy: Implications for Cordilleran Orogenesis

One of the most striking features of our model is a conspicuous orogen-parallel anisotropy in the lower crust beneath the Canadian Cordillera and the neighboring foreland belt. Possible sources for crustal anisotropy include stress-aligned shape-preferred orientation (SPO) of cracks in the upper crust and LPO of anisotropic crustal minerals (e.g., mica and amphibole) in the middle to lower crust due to intensive, regionally coherent strain [Crampin *et al.*, 1984]. This NW–SE trending fabric is perpendicular to the regional maximum horizontal

Figure 6. Inversion results of isotropic phase velocities and azimuthal anisotropy for the study region. The isotropic phase velocity is plotted relative to the average phase velocity at the corresponding period. The black bars show the peak-to-peak magnitude and fast-propagation direction of azimuthal anisotropy.

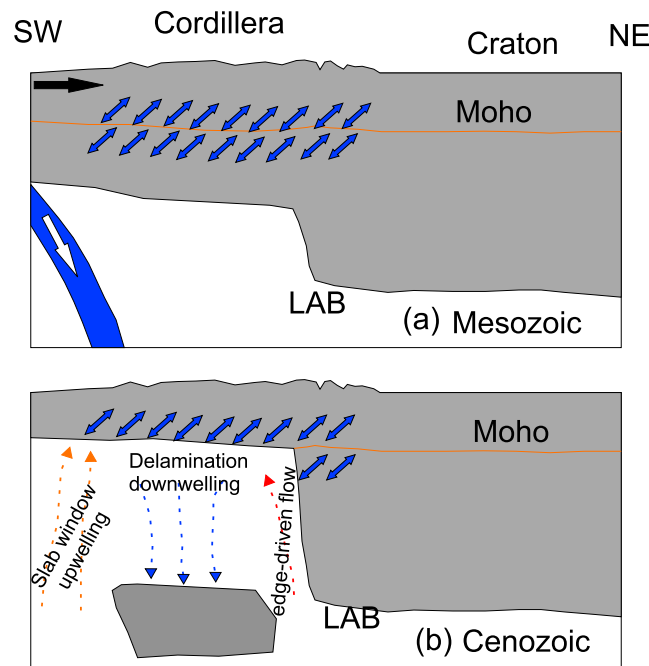


Figure 8. A possible scenario for the formation of layered anisotropy in the Cordillera. (a) During the Mesozoic Cordilleran orogenesis, the pervasive orogeny-parallel deformation fabrics (NW–SE) formed in the lower crust beneath the Cordillera and foreland belt, possibly as a result of channel flow. Double arrows indicate flow perpendicular to the plane of the section. (b) During the Cenozoic, the complex interaction of vertical mantle flow caused by lithospheric delamination, slab window, and step change of lithospheric thickness may result in the observed low azimuthal anisotropy in the asthenosphere.

compressional stress [Reiter *et al.*, 2014], ruling out SPO due to the contemporary stress field. On the other hand, the strong orogen-parallel anisotropy in the lower crust may be caused by LPO of amphibole and/or mica formed during the formation of the Cordillera. Since the Jurassic, Cordilleran orogenesis has dominated the tectonic evolution to the west, which was initiated by the oblique plate convergence along the western margin of North America [Cook, 1995]. The accompanying compressional stress field that is perpendicular to the strike of the orogen may have modulated the ductile deformation of the lower crust and uppermost mantle in the form of mountain-parallel material flow [Meissner *et al.*, 2002]. We therefore interpret this feature to reflect LPO of amphibole and/or mica in the lower crust resulting from persistent orogen-parallel, lower-crustal channel flow [Meissner *et al.*, 2002; Royden *et al.*, 1997] coeval with formation of the Canadian Cordillera (Figure 8a). This model is consistent with the observed positive radial anisotropy beneath the Cordillera [Dalton and Gaherty, 2013].

Similar orogen-parallel anisotropy has been documented in several previous studies. For instance, using ambient noise tomography, Fry *et al.* [2010] imaged pervasive orogen-parallel anisotropy above 30 km depth in the central Alps. Using surface wave tomography, Deschamps *et al.* [2008] found that directions of fast wave propagation in the upper lithosphere (30–70 km depths) beneath the east central United States are parallel to the Grenville and Appalachian fronts. The pervasive orogen-parallel deformation fabrics observed by these studies suggest that broad continuously distributed deformation may be a common phenomenon in continental collision zones, which occurs not only in the upper crust [Zhang *et al.*, 2004] but also in the middle to lower crust and uppermost mantle likely through ductile flow [Royden *et al.*, 1997].

5.2. Apparent Weak Asthenospheric Anisotropy Below the Cordillera

Another pronounced feature of our results is a region of low-to-zero azimuthal anisotropy beneath the southern Canadian Cordillera at periods large than 70 s. The depth location of this zone of weak azimuthal anisotropy is probably within the asthenosphere because of the unusually thin lithosphere beneath the interior of the southern Canadian Cordillera [Bao *et al.*, 2014; Miller and Eaton, 2010; Yuan and Romanowicz, 2010]. The weak azimuthal anisotropy from our surface wave tomography agrees well with the null-splitting measurements of SKS splitting [Currie *et al.*, 2004] (Figure 1). Possible interpretations of this feature include (1) an area of stagnant flow, (2) asthenospheric flow that is heterogeneous at scale lengths below the resolution of method, and (3) flow that is predominantly vertical (either upward or downward), since our method is insensitive to seismic anisotropy induced by vertical flow. In the case of small-scale heterogeneous flow patterns, our method tends to average out azimuthal anisotropy, even if the degree of anisotropy within individual flow cells is relatively strong.

Possible causes for small-scale heterogeneous mantle flow (including vertical flow) in this region include the delamination of lithospheric mantle, slab window, and edge-driven convection [Gu *et al.*, 2011]. Based on surface wave tomography and thermochronological data, the rapid uplift of the southern Canadian

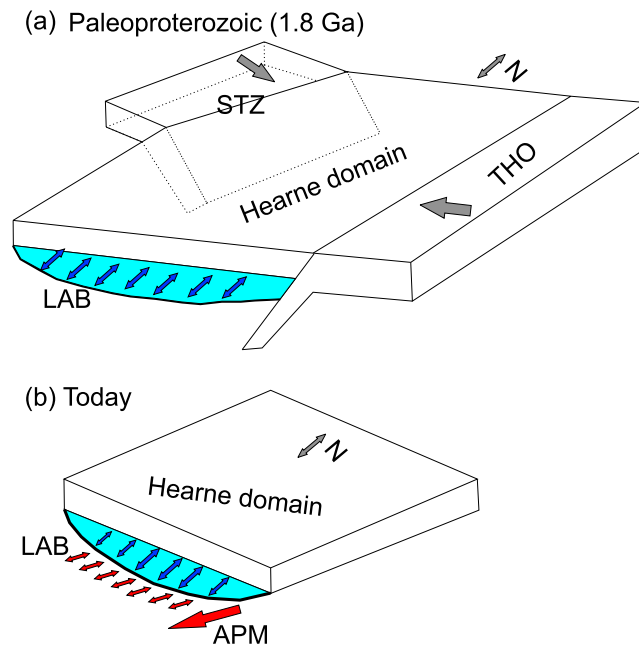


Figure 9. A possible model for the origin of anisotropy layering in the cratonic region. (a) During the Paleoproterozoic assembly of western Laurentia, synchronous inward dipping subductions along the Trans-Hudson orogen and the Snowbird tectonic zone (STZ) formed a tectonic vise, which caused the basal accretion of the original cratonic lithosphere and the formation of N-S anisotropic fabrics beneath the Hearne domain (blue double arrows). (b) At present, the motion of the North American plate (red big arrow) induces shear deformation in the asthenosphere, giving rise to the NE-SW trending anisotropy (red double arrows).

asthenospheric upwelling, and edge-driven convection may have resulted in the anisotropy low (Figure 8b), similar to interpretations in other regions [e.g., Bastow et al., 2015].

5.3. Multiple Layers of Anisotropy Beneath Western Laurentia

Depth-variant azimuthal anisotropy is apparent in parts of the craton. At periods sampling the cratonic lithosphere (40–120 s), the dominant directions of fast wave propagation in the southeastern part of our study region are N-S. By contrast, at a period of 150 s sampling the lower lithosphere and asthenosphere, the fast wave azimuths change toward NE–SW, which is close to the absolute plate motion of the North American plate and the fast wave azimuth obtained by previous SKS splitting measurements [Courtier et al., 2010; Gu et al., 2011; Shragge et al., 2002]. Previous shear wave splitting measurements have also suggested the existence of multiple layers of anisotropy in this region. Significant azimuthal variations in the shear wave splitting parameters with a 90° periodicity were observed in the two stations (WALA and EDM, as shown in Figure 1), which is indicative of layered anisotropy [Currie et al., 2004]. Further modeling by Currie et al. [2004] suggested an upper layer of anisotropy with a nearly N-S fast direction (N12°E) and a lower layer of anisotropy with a fast direction of N81°E, which is broadly coincident with the depth variation of Rayleigh wave azimuthal anisotropy revealed in this study. If we assume an average shear velocity of ~4.7 km/s [Bao and Eaton, 2015] and anisotropy of ~3% for the lithospheric mantle, the inferred delay time of ~1.4 s for the upper layer [Currie et al., 2004] requires a layer of thickness ~220 km [Silver, 1996], broadly consistent with the thick cratonic lithosphere in this region [Bao and Eaton, 2015]. Since the magnitude of anisotropy in the asthenosphere at great depth is not well constrained by this study, we use an average anisotropy of 4.5% to estimate the thickness of the lower layer. Thus, the inferred delay time of ~2.0 s for the lower layer [Currie et al., 2004] requires an anisotropic layer of thickness ~208 km, suggesting a significant contribution of the sublithospheric mantle to the measured SKS splitting. Multiple layers of anisotropy beneath the North American craton have also been imaged by other continental- and regional-scale

Cordillera has been interpreted to have initiated from lithospheric delamination commencing about 55 Ma [Bao et al., 2014]. A lithospheric downwelling model [West et al., 2009] has also been proposed to explain the apparent absence of anisotropic fabric detected by SKS splitting in the Great Basin region of the western United States, an intriguing phenomenon with multiple explanations [e.g., Zandt and Humphreys, 2008]. On the other hand, slab window-induced vertical asthenospheric flow in the Cenozoic has been proposed to explain the null splitting observation (weak azimuthal anisotropy) [Currie et al., 2004; Zandt et al., 2009] and intraplate volcanism [Thorkelson et al., 2011] in the Canadian Cordillera. Upward or downward flow component of the edge-driven convection [Hardebol et al., 2012] caused by the sharp change of lithospheric thickness from the Cordillera to the craton may further contribute to the weak azimuthal anisotropy. Thus, some combinations of lithospheric delamination,

seismic studies [Darbyshire and Lebedev, 2009; Darbyshire et al., 2015; Yuan and Romanowicz, 2010], with an upper layer of frozen anisotropy and a lower layer of anisotropy caused by recent and present-day mantle flow.

The N-S fossilized anisotropy in the upper to middle lithosphere mantle beneath the craton region is probably linked to the assembly of western Laurentia during the Paleoproterozoic, as this region has since been tectonically quiescent (Figure 9). A tectonic “vise” model composed of coeval inward dipping subductions along the Snowbird Tectonic Zone and the Trans-Hudson Orogen has been invoked to describe the assembly of western Laurentia [Ross et al., 2000] (Figure 9). In this model, the cratonic lithosphere experienced pervasive collisional reworking and thickening [Bao and Eaton, 2015]. The Trans-Hudson Orogen has been considered as a tectonic event comparable to the Himalayan-Tibetan orogen in terms of spatial extent and deformation rate [Eaton and Darbyshire, 2010; St-Onge et al., 2006], which would likely cause plate-scale deformation fabrics [Bastow et al., 2011]. The coherent N-S anisotropic fabrics revealed here generally follow the trending of the Trans-Hudson Orogen to the east, indicating that the lithospheric thickening during the assembly of western Laurentia was also collocated with the formation of distinct deformation fabrics (Figure 9). Similar episodic formation model for cratonic lithosphere has previously been proposed for other parts of the North American craton [Darbyshire et al., 2013; Yuan and Romanowicz, 2010]. For example, Darbyshire et al. [2013] found that anisotropic fabrics of the lower lithosphere at depths >150 km beneath the Hudson Bay region show a distinct pattern closely resembling the subsurface geometry of the Trans-Hudson Orogen, suggesting that the basal layer accreted to the old lithosphere following the main phase of the Trans-Hudson orogeny.

6. Conclusions

The depth distribution of azimuthal anisotropy in western Canada is elucidated in this study through regional Rayleigh wave tomography. Our azimuthally anisotropic phase velocity maps provide evidence for a pronounced orogen-parallel lower crustal anisotropy in the Cordillera and the adjacent foreland. By analogy with studies of other orogenic belts, this fabric is interpreted as lower crustal channel flow that formed as a result of Laramide deformation. A zone of low-to-zero azimuthal anisotropy in the southern part of the Cordillera provides evidence for small-scale heterogeneous asthenospheric flow patterns, possibly associated with vertical flow. This may be caused by the combined effects of the Juan de Fuca slab window, lithospheric delamination, and edge-driven convection. To the east, the adjacent craton is characterized by two layers of anisotropy with N-S seismic fast azimuth at periods of <120 s and NE-SW fast azimuth at a period of 150 s. This pattern is consistent with SKS splitting observation and is interpreted to represent a transition from frozen anisotropy in the cratonic lithosphere to underlying asthenospheric flow that is driven by plate motion. Fossil deformation fabrics within the cratonic lithosphere are likely to represent relict features from collisional assembly of western Laurentia.

Acknowledgments

Seismic data were obtained from the Incorporated Research Institutions for Seismology Data Management Center (www.iris.edu) and the Canadian National Data Center (<http://www.earthquakescanada.nrcan.gc.ca/index-eng.php>). This study was funded by a grant to DWE from the Natural Sciences and Engineering Research Council of Canada (NSERC). Most figures were produced using Generic Mapping Tools (GMT) [Wessel and Smith, 1998]. We appreciate Fiona A. Darbyshire for giving instruction on anisotropic tomography. We thank the team of CRANE project for the hard work to collect their data. We are grateful to the Editors and anonymous referees for their constructive comments to improve this paper.

References

- Adam, J. M. C., and S. Lebedev (2012), Azimuthal anisotropy beneath southern Africa from very broad-band surface-wave dispersion measurements, *Geophys. J. Int.*, *191*(1), 155–174, doi:10.1111/j.1365-246X.2012.05583.x.
- Babuška, V., and J. Plomerová (2006), European mantle lithosphere assembled from rigid microplates with inherited seismic anisotropy, *Phys. Earth Planet. Inter.*, *158*, 264–280.
- Bao, X., and D. W. Eaton (2015), Large variations in lithospheric thickness of western Laurentia: Tectonic inheritance or collisional reworking? *Precambrian Res.*, *266*, 579–586, doi:10.1016/j.precamres.2015.05.010.
- Bao, X., M. Xu, L. Wang, N. Mi, D. Yu, and H. Li (2011), Lithospheric structure of the Ordos Block and its boundary areas inferred from Rayleigh wave dispersion, *Tectonophysics*, *499*(1–4), 132–141.
- Bao, X., X. Song, M. Xu, L. Wang, X. Sun, N. Mi, D. Yu, and H. Li (2013), Crust and upper mantle structure of the North China Craton and the NE Tibetan Plateau and its tectonic implications, *Earth Planet. Sci. Lett.*, *369*, 129–137.
- Bao, X., D. W. Eaton, and B. Guest (2014), Plateau uplift in western Canada caused by lithospheric delamination along a craton edge, *Nat. Geosci.*, *7*(11), 830–833, doi:10.1038/ngeo2270.
- Bascou, J., G. Delpech, A. Vauchez, B. N. Moine, J. Y. Cottin, and G. Barruol (2008), An integrated study of microstructural, geochemical, and seismic properties of the lithospheric mantle above the Kerguelen plume (Indian Ocean), *Geochem. Geophys. Geosyst.*, *9*, Q04036, doi:10.1029/2007GC001879.
- Bastow, I. D., D. A. Thompson, J. Wookey, J.-M. Kendall, G. Helffrich, D. B. Snyder, D. W. Eaton, and F. A. Darbyshire (2011), Precambrian plate tectonics: Seismic evidence from northern Hudson Bay, Canada, *Geology*, *39*, 91–94.
- Bastow, I. D., J. Julia, A. F. do Nascimento, R. A. Fuck, T. L. Buckthorp, and J. J. McClellan (2015), Upper mantle anisotropy of the Borborema Province, NE Brazil: Implications for intra-plate deformation and sub-cratonic asthenospheric flow, *Tectonophysics*, *657*, 81–93.
- Bastow, I., T. Owens, G. Helffrich, and J. Knapp (2007), Spatial and temporal constraints on sources of seismic anisotropy: Evidence from the Scottish highlands, *Geophys. Res. Lett.*, *34*, L05305, doi:10.1029/2006GL028911.

- Boerner, D. E., R. D. Kurtz, J. A. Craven, G. M. Ross, F. W. Jones, and W. J. Davis (1999), Electrical conductivity in the Precambrian lithosphere of western Canada, *Science*, *283*(5402), 668–670.
- Bokelmann, G. H. R., and P. G. Silver (2000), Mantle variation within the Canadian Shield: Travel times from the portable broadband Archean-Proterozoic transect, *J. Geophys. Res.*, *105*, 579–605.
- Bystricky, M., K. Kunze, L. Burlini, and J.-P. Burg (2000), High shear strain of olivine aggregates: Rheological and seismic consequences, *Science*, *290*(5496), 1564–1567.
- Cassidy, J. F. (1995), Review: Receiver function studies in the southern Canadian Cordillera, *Can. J. Earth Sci.*, *32*(10), 1514–1519.
- Chen, H., L. Zhu, Q. Ye, Q. Wang, Y. Yang, and P. Zhang (2015a), Azimuthal anisotropy of the crust and uppermost mantle in northeast North China Craton from inversion of Rayleigh wave phase velocity, *Geophys. J. Int.*, *202*(1), 624–639.
- Chen, Y., Y. J. Gu, R. M. H. Dokht, and M. D. Sacchi (2015b), Crustal imprints of Precambrian orogenesis in western Laurentia, *J. Geophys. Res. Solid Earth*, *120*, 6993–7012, doi:10.1002/2014JB011353.
- Cook, F. A. (1995), Lithospheric processes and products in the southern Canadian Cordillera: A Lithoprobe perspective, *Can. J. Earth Sci.*, *32*(10), 1803–1824.
- Courtier, A. M., J. B. Gaherty, J. Revenaugh, M. G. Bostock, and E. J. Garnero (2010), Seismic anisotropy associated with continental lithosphere accretion beneath the CANOE array, northwestern Canada, *Geology*, *38*(10), 887–890.
- Crampin, S., E. M. Chesnokov, and R. G. Hipkin (1984), Seismic anisotropy—The state of the art: II, *Geophys. J. R. Astron. Soc.*, *76*(1), 1–16.
- Currie, C. A., J. F. Cassidy, R. D. Hyndman, and M. G. Bostock (2004), Shear wave anisotropy beneath the Cascadia subduction zone and western North American craton, *Geophys. J. Int.*, *157*(1), 341–353.
- Dalton, C. A., and J. B. Gaherty (2013), Seismic anisotropy in the continental crust of northwestern Canada, *Geophys. J. Int.*, *193*(1), 338–348.
- Dalton, C. A., J. B. Gaherty, and A. M. Courtier (2011), Crustal V5 structure in northwestern Canada: Imaging the Cordillera-craton transition with ambient noise tomography, *J. Geophys. Res.*, *116*, B12315, doi:10.1029/2011JB008499.
- Darbyshire, F. A., and S. Lebedev (2009), Rayleigh wave phase-velocity heterogeneity and multilayered azimuthal anisotropy of the Superior Craton, Ontario, *Geophys. J. Int.*, *176*(1), 215–234.
- Darbyshire, F. A., D. W. Eaton, and I. D. Bastow (2013), Seismic imaging of the lithosphere beneath Hudson Bay: Episodic growth of the Laurentian mantle keel, *Earth Planet. Sci. Lett.*, *373*, 179–193.
- Darbyshire, F. A., I. D. Bastow, A. M. Forte, T. E. Hobbs, A. Calvel, A. Gonzalez-Monteza, and B. Schow (2015), Variability and origin of seismic anisotropy across eastern Canada: Evidence from shear-wave splitting measurements, *J. Geophys. Res. Solid Earth*, *120*, 8404–8421, doi:10.1002/2015JB012228.
- Debayle, E., B. Kennett, and K. Priestley (2005), Global azimuthal seismic anisotropy and the unique plate-motion deformation of Australia, *Nature*, *433*(7025), 509–512.
- Deschamps, F., S. Lebedev, T. Meier, and J. Trampert (2008), Stratified seismic anisotropy reveals past and present deformation beneath the east-central United States, *Earth Planet. Sci. Lett.*, *274*(3–4), 489–498.
- Eaton, D., and F. Darbyshire (2010), Lithospheric architecture and tectonic evolution of the Hudson Bay region, *Tectonophysics*, *480*, 1–22.
- Eaton, D., A. Frederiksen, and S.-K. Miong (2004), Shear-wave splitting observations in the lower Great Lakes region: Evidence for regional anisotropic domains and keel-modified asthenospheric flow, *Geophys. Res. Lett.*, *31*, L07610, doi:10.1029/2004GL019438.
- England, P., and G. Houseman (1986), Finite strain calculations of continental deformation. 2. Comparison with the India-Asia collision zone, *J. Geophys. Res.*, *91*, 3664–3676, doi:10.1029/JB091ib03p03664.
- Forsyth, D. W. (1975), The early structural evolution and anisotropy of the oceanic upper mantle, *Geophys. J. R. Astron. Soc.*, *43*(1), 103–162.
- Fry, B., F. Deschamps, E. Kissling, L. Stehly, and D. Giardini (2010), Layered azimuthal anisotropy of Rayleigh wave phase velocities in the European Alpine lithosphere inferred from ambient noise, *Earth Planet. Sci. Lett.*, *297*(1–2), 95–102.
- Gaherty, J. B. (2004), A surface wave analysis of seismic anisotropy beneath eastern North America, *Geophys. J. Int.*, *158*(3), 1053–1066.
- Gripp, A. E., and R. G. Gordon (2002), Young tracks of hotspots and current plate velocities, *Geophys. J. Int.*, *150*, 321–361.
- Gu, Y. J., and L. Shen (2015), Noise correlation tomography of Southwest Western Canada Sedimentary Basin, *Geophys. J. Int.*, *202*(1), 142–162.
- Gu, Y. J., A. Okeler, L. Shen, and S. Contenti (2011), The Canadian Rockies and Alberta Network (CRANE): New constraints on the Rockies and western Canada sedimentary basin, *Seismol. Res. Lett.*, *82*(4), 575–588.
- Gu, Y. J., Y. Zhang, M. D. Sacchi, Y. Chen, and S. Contenti (2015), Sharp mantle transition from cratons to Cordillera in southwestern Canada, *J. Geophys. Res. Solid Earth*, *120*, 5051–5069, doi:10.1002/2014JB011802.
- Hardebol, N. J., R. N. Pysklywec, and R. Stephenson (2012), Small-scale convection at a continental back-arc to craton transition: Application to the southern Canadian Cordillera, *J. Geophys. Res.*, *117*, B01408, doi:10.1029/2011JB008431.
- Hoffman, P. F. (1988), United plates of America, the birth of a craton: Early proterozoic assembly and growth of Laurentia, *Ann. Rev. Earth Planet. Sci.*, *16*(1), 543–603.
- Holtzman, B. K., D. L. Kohlstedt, M. E. Zimmerman, F. Heidelbach, T. Hiraga, and J. Hustoft (2003), Melt segregation and strain partitioning: Implications for seismic anisotropy and mantle flow, *Science*, *301*(5637), 1227–1230.
- Ismail, W. B., and D. Mainprice (1998), An olivine fabric database: An overview of upper mantle fabrics and seismic anisotropy, *Tectonophysics*, *296*(1–2), 145–157.
- Jung, H., and S.-I. Karato (2001), Water-induced fabric transitions in olivine, *Science*, *293*(5534), 1460–1463.
- Kao, H., Y. Behr, C. A. Currie, R. Hyndman, J. Townend, F.-C. Lin, M. H. Ritzwoller, S.-J. Shan, and J. He (2013), Ambient seismic noise tomography of Canada and adjacent regions: Part I. Crustal structures, *J. Geophys. Res. Solid Earth*, *118*, 5865–5887, doi:10.1002/2013JB010535.
- Lebedev, S., J. Boonen, and J. Trampert (2009), Seismic structure of Precambrian lithosphere: New constraints from broad-band surface-wave dispersion, *Lithos*, *109*, 96–111.
- Li, A., D. W. Forsyth, and K. M. Fischer (2003), Shear velocity structure and azimuthal anisotropy beneath eastern North America from Rayleigh wave inversion, *J. Geophys. Res.*, *108*(B8), 2362, doi:10.1029/2002JB002259.
- Lin, F.-C., M. H. Ritzwoller, Y. Yang, M. P. Moschetti, and M. J. Fouch (2011), Complex and variable crustal and uppermost mantle seismic anisotropy in the western United States, *Nat. Geosci.*, *4*(1), 55–61.
- Marone, F., and B. Romanowicz (2007), The depth distribution of azimuthal anisotropy in the continental upper mantle, *Nature*, *447*(7141), 198–201.
- Meade, B. J. (2007), Present-day kinematics at the India-Asia collision zone, *Geology*, *35*(1), 81–84.
- Meissner, R., W. D. Mooney, and I. Artemieva (2002), Seismic anisotropy and mantle creep in young orogens, *Geophys. J. Int.*, *149*, 1–14.
- Mercier, J. P., M. G. Bostock, J. F. Cassidy, K. Dueker, J. B. Gaherty, E. J. Garnero, J. Revenaugh, and G. Zandt (2009), Body-wave tomography of western Canada, *Tectonophysics*, *475*(3–4), 480–492.
- Miller, M. S., and D. W. Eaton (2010), Formation of cratonic mantle keels by arc accretion: Evidence from S receiver functions, *Geophys. Res. Lett.*, *37*, L18305, doi:10.1029/2010GL044366.
- Molnar, P. (1988), Continental tectonics in the aftermath of plate tectonics, *Nature*, *335*(6186), 131–137.

- Montagner, J.-P., and H.-C. Nataf (1986), A simple method for inverting the azimuthal anisotropy of surface waves, *J. Geophys. Res.*, *91*, 511–520, doi:10.1029/JB091iB01p00511.
- Montagner, J.-P., and T. Tanimoto (1991), Global upper mantle tomography of seismic velocities and anisotropies, *J. Geophys. Res.*, *96*, 20,337–20,351.
- Nataf, H. C., I. Nakanishi, and D. L. Anderson (1984), Anisotropy and shear-velocity heterogeneities in the upper mantle, *Geophys. Res. Lett.*, *11*, 109–112.
- Nicolas, A., and N. I. Christensen (1987), Formation of anisotropy in upper mantle peridotites—A review, in *Composition, Structure and Dynamics of the Lithosphere-Asthenosphere System*, pp. 111–123, AGU, Washington, D. C., doi:10.1029/GD016p0111.
- Nieuwenhuis, G., M. J. Unsworth, D. Pana, J. Craven, and E. Bertrand (2014), Three-dimensional resistivity structure of Southern Alberta, Canada: Implications for Precambrian tectonics, *Geophys. J. Int.*, *197*(2), 838–859.
- Paige, C. C., and M. A. Saunders (1982), LSQR: An algorithm for sparse linear equations and sparse least squares, *TOMS*, *8*(1), 43–71.
- Pawlak, A., D. W. Eaton, F. Darbyshire, S. Lebedev, and I. D. Bastow (2012), Crustal anisotropy beneath Hudson Bay from ambient noise tomography: Evidence for post-orogenic lower-crustal flow?, *J. Geophys. Res.*, *117*, B08301, doi:10.1029/2011JB009066.
- Pedersen, H. A., M. Bruneton, and V. Maupin (2006), Lithospheric and sublithospheric anisotropy beneath the Baltic shield from surface-wave array analysis, *Earth Planet. Sci. Lett.*, *244*(3–4), 590–605.
- Plomerová, J., D. Kouba, and V. Babuška (2002), Mapping the lithosphere-asthenosphere boundary through changes in surface-wave anisotropy, *Tectonophysics*, *358*(1–4), 175–185.
- Reiter, K., O. Heidbach, D. Schmitt, K. Haug, M. Ziegler, and I. Moeck (2014), A revised crustal stress orientation database for Canada, *Tectonophysics*, *636*, 111–124.
- Ross, G. M. (2002), Evolution of Precambrian continental lithosphere in western Canada: Results from Lithoprobe studies in Alberta and beyond, *Can. J. Earth Sci.*, *39*(3), 413–437.
- Ross, G. M., R. R. Parrish, M. E. Villeneuve, and S. A. Bowring (1991), Geophysics and geochronology of the crystalline basement of the Alberta Basin, western Canada, *Can. J. Earth Sci.*, *28*(4), 512–522.
- Ross, G. M., D. W. Eaton, D. E. Boerner, and W. Miles (2000), Tectonic entrapment and its role in the evolution of continental lithosphere: An example from the Precambrian of western Canada, *Tectonics*, *19*, 116–134, doi:10.1029/1999TC900047.
- Royden, L. H., B. C. Burchfiel, R. W. King, E. Wang, Z. Chen, F. Shen, and Y. Liu (1997), Surface deformation and lower crustal flow in eastern Tibet, *Science*, *276*(5313), 788–790.
- Savage, M. K. (1999), Seismic anisotropy and mantle deformation: What have we learned from shear wave splitting?, *Rev. Geophys.*, *37*, 65–106.
- Shearer, P. M., and J. A. Orcutt (1986), Compressional and shear wave anisotropy in the oceanic lithosphere—The Ngendei seismic refraction experiment, *Geophys. J. Int.*, *87*(3), 967–1003.
- Shragge, J., M. G. Bostock, C. G. Bank, and R. M. Ellis (2002), Integrated teleseismic studies of the southern Alberta upper mantle, *Can. J. Earth Sci.*, *39*(3), 399–411.
- Silver, P. G. (1996), Seismic anisotropy beneath the continents: Probing the Depths of Geology, *Ann. Rev. Earth Planet. Sci.*, *24*(1), 385–432.
- Smith, M. L., and F. A. Dahlen (1973), The azimuthal dependence of love and Rayleigh wave propagation in a slightly anisotropic medium, *J. Geophys. Res.*, *78*, 3321–3333, doi:10.1029/JB078i017p03321.
- St-Onge, M. R., M. P. Searle, and N. Wodicka (2006), Trans-Hudson orogen of north America and Himalaya-Karakoram-Tibetan orogen of Asia: Structural and thermal characteristics of the lower and upper plates, *Tectonics*, *25*, TC4006, doi:10.1029/2005TC001907.
- Tapponnier, P., G. Peltzer, A. Y. Le Dain, R. Armijo, and P. Cobbold (1982), Propagating extrusion tectonics in Asia: New insights from simple experiments with plasticine, *Geology*, *10*(12), 611–616.
- Tapponnier, P., X. Zhiqin, F. Roger, B. Meyer, N. Arnaud, G. Wittlinger, and Y. Jingsui (2001), Oblique stepwise rise and growth of the Tibet plateau, *Science*, *294*(5547), 1671–1677.
- Thorkelson, D. J., J. K. Madsen, and C. L. Sluggett (2011), Mantle flow through the Northern Cordilleran slab window revealed by volcanic geochemistry, *Geology*, *39*(3), 267–270.
- Vinnik, L. P., L. I. Makeyeva, A. Milev, and A. Y. Usenko (1992), Global patterns of azimuthal anisotropy and deformations in the continental mantle, *Geophys. J. Int.*, *111*(3), 433–447.
- Wessel, P., and W. H. F. Smith (1998), New, improved version of the Generic Mapping Tools Released, *Eos Trans. AGU*, *79*(47), 579.
- West, J. D., M. J. Fouch, J. B. Roth, and L. T. Elkins-Tanton (2009), Vertical mantle flow associated with a lithospheric drip beneath the Great Basin, *Nat. Geosci.*, *2*(6), 439–444.
- Xu, Z., X. Song, and S. Zheng (2013), Shear velocity structure of crust and uppermost mantle in China from surface wave tomography using ambient noise and earthquake data, *Earthquake Sci.*, *26*(5), 267–281.
- Yao, H. J., R. D. van der Hilst, and M. V. de Hoop (2006), Surface-wave array tomography in SE Tibet from ambient seismic noise and two-station analysis—I. Phase velocity maps, *Geophys. J. Int.*, *166*(2), 732–744.
- Yao, H., R. D. van der Hilst, and J.-P. Montagner (2010), Heterogeneity and anisotropy of the lithosphere of SE Tibet from surface wave array tomography, *J. Geophys. Res.*, *115*, B12307, doi:10.1029/2009JB007142.
- Yuan, H., and B. Romanowicz (2010), Lithospheric layering in the North American craton, *Nature*, *466*(7310), 1063–1068.
- Zandt, G., A. M. Frassetto, J. F. Cassidy, and M. G. Bostock (2009), Regional variations of mantle anisotropy across the Canadian Cordillera from teleseismic shear-wave splitting, Abstract #S11A-1685 presented at 2009 Fall Meeting, AGU.
- Zhang, P.-Z., et al. (2004), Continuous deformation of the Tibetan Plateau from Global Positioning System data, *Geology*, *32*(9), 809–812.
- Zhang, S., and S.-I. Karato (1995), Lattice preferred orientation of olivine aggregates deformed in simple shear, *Nature*, *375*, 774–777.
- Zandt, G., and E. Humphreys (2008), Toroidal mantle flow through the western US slab window, *Geology*, *36*(4), 295–298.